Experimental characterization and micromechanical modeling of the elastic response of the human humerus under bending impact

Jamila Rahmoun, Hakim Naceur, Hervé Morvan, Pascal Drazetic, Christian Fontaine, P.-E. Mazeran

Version of Record: https://www.sciencedirect.com/science/article/pii/S0928493119301870
Manuscript_2bc49a971cd8dcc606bbb30b56e66b1a

Experimental characterization and micromechanical modeling of the elastic response of the human humerus under bending impact

J. Rahmoun[a,*], H. Naceur[a], H. Morvan[a], P. Drazetic[a], C. Fontaine[b], P.E. Mazeran[c]

[a] *Univ. Polytechnique Hauts-de-France, CNRS, INSA Hauts-de-France, UMR 8201-LAMIH, F-59313 Valenciennes, France*
[b] *Univ. Lille 2, Faculté de medecine, Laboratoire d'Anatomie, CHRU de Lille, F-59045 Lille, France*
[c] *Univ. de Technologie de Compiègne, CNRS, FRE 2012-ROBERVAL, F-60205 Compiègne, France*

Abstract

This paper investigates the characterization and numerical modeling of the elastic behavior of the human humerus bone using a recently developed micromechanical approach coupled to nanoindentation measurements. At first, standard three-point bending experiments were conducted under low static loading, using several humerus diaphysis in order to identify the apparent elastic modulus of the bone in static regime. Then, a drop tower impact experiment was used on the same set of humerus diaphysis specimens, in order to assess the elastic modulus in dynamic regime. These measurements will be used as reference bases for comparison purpose. The originality of this work, lies in the coupling between a two-phase micromechanical approach based on Mori-Tanaka homogenization scheme for cylindrical voids and nanoindentation measurements of the elastic modulus of the bone matrix phase. This model has been implemented using a user defined material subroutine VMAT in ABAQUS© Explicit code. The bone mechanical response prediction using the proposed methodology was validated against previous standard experimental data. Finally, it was shown that the numerical predictions are consistent with the physical measurements obtained on human humerus via the good estimation of the ultimate impact load.

Keywords: Human humerus bone, micromechanics, nanoindentation, drop tower impact, Finite Element.

1. Introduction

With the growing deployment of airbag protection systems by cars manufacturers to increase passengers safety, it has been noticed an increased emphasis on the study of the upper extremity injuries in the automotive environment [17]. These research studies include the investigations on injuries of the upper extremities, in particular humeri, from deploying airbags. The Humerus is the second most common long bone diaphyses known. Its bone functional adaptation to strain is achieved by the addition and redistribution of tissue [32]. Moreover, the humeral bone is an hierarchical material whose architecture differs at each level

*Corresponding author : jamila.rahmoun@uphf.fr, Phone +33 327 511 412

of hierarchy and whose mechanical properties can vary considerably, even on the same specimen, due to the bone heterogeneity. Different approaches have been performed to account for the multi-scale nature of bone. Homogenization techniques have been developed to model its elasticity and fracture risk [21]. Interestingly, continuum micromechanical based approaches allow the modeling of the bone anisotropic mechanical properties [12; 27]. The predictive potential of the so-called micromechanical formulation has been shown using physically and statistically independent sets of experiments.

For the determination of the humerus mechanical properties and its integration in numerical models, characterization tests of humerus bone are needed. Moreover, global tests performed on an humerus are also required for the validation of bone models with respect to the experimental data. Concerning the studies investigating the material properties of the humerus bone, we can cite the study of Singh *et al.* [33] who supplied the needed mechanical parameters given by different global tests (three-point bending, fracture toughness, and axial compression). Hoffler *et al.* [15] performed nanoindentation tests on lamellae level and found that the elastic modulus and hardness of human bone tissue depend strongly on tissue type, anatomical location and individual. Nevertheless, most of the existing studies concerning global tests on humerus are mainly done in quasi-static conditions [5; 16]. Impact testing provides information about the response of a material to a dynamic load. This knowledge is essential for materials whose properties are time-dependent, e.g. exhibit viscoelasticity or poroelasticity. Most biological materials have such properties and yet their responses at loading rates that may be found during rapid physiological activities, or when subject to traumatic forces such as during falls or accidents, are still not well understood. Only in few studies, the humerus has been loaded at level of velocity close to those to which the humerus bone could be subjected during a car accident. We can cite the work of Lebarbé *et al.* [19] who investigates the human shoulder response to lateral impact at intermediate velocities. The obtained shoulder injury mechanism appeared to be similar to those observed in the automotive field.

The aim of the present paper is to propose a micromechanical based approach for the accurate characterization and modeling of the elastic behavior of the human humerus under bending impact. The present micromechanical model [30; 31; 36] is based on the coupling between the Mori-Tanaka homogenization scheme [24] for the estimation of the elastic properties of the humeral cortical bone, and a Finite Element model at the macro-level for the prediction of the global humerus diaphysis elastic response. The proposed procedure consists in two stages: at first, local measurements of the bone material properties were performed thanks to nanoindentation tests using small specimens extracted directly from the same humerus diaphysis. Once the bone matrix material parameters (Young's modulus, porosity) were determined, a bending impact test was performed using a solid-shell finite element model [8; 26] to validate the global response of the modeled humain humerus diaphysis.

2. Experimental characterization of the mechanical response of the human humerus diaphysis under bending loading

2.1. Three points bending tests of the humerus

2.1.1. Sample preparation and instrumentation

Five fresh left humeri were obtained from human cadavers with an average age of 68.6 ± 7.4 years and an average body height of 180 ± 7.8 *cm*. The humerus bones were supplied by the Department of Anatomy at Lille University School of Medicine in accordance with French regulations. The average length of these specimens was 345 ± 14.1 *mm* with an average mass of 226 ± 56.8 *g*. Each specimen has been submitted to a virological and serological analysis to ensure that they do not exhibit any bone disease on radiographic examination. All specimens were scanned using a medical scanner. These acquisitions were performed to extract the digital geometry data and saved using the stereolithography (STL) standard format then exported to a Computer Aided Design (CAD) workstation. Finally, the specimens were embalmed using a solution composed of methanol (35%), phenol (10%), glycerin (20%) and distilled water (35%) and stored at 4^oC until the beginning of experiments. Several studies [34; 35; 11] have investigated the effects of embalming bones regarding their mechanical properties. It be founded no or little effect after short to intermediate storage periods on the elastic properties of the human bones measured by experimental tests (see [34]).

Each humerus was prepared 24 hours before the starting of experiments in order to fix it rigidly inside two aluminum prismatic brackets (see Figure 1*b*) which were positioned onto a flat support to ensure their parallelism. One of the metallic brackets was maintained, while the other was free to slide in order to adapt it to the desired length of the bone. For each humerus, four positioning screws (Figure 1*b*) were used to help maintaining fixed the epiphyses and the lateral epicondyle of the humerus to the brackets. The system humerus-brackets was first positioned vertically and a FASTCAST© Polyurethane resin (type F14-F15 from AXSON Company) was poured into the lower bracket. Three hours later (recommended resin drying duration), the humerus-brackets system was flipped and the same operation was done for the other bracket side. The screws are then removed and the system humerus-bracket was separated from the straight support and placed in a cold room.

Two hours before the starting of experiments, five strain gages (Y series 1-LY41-3/350 from HBM) were glued on the humerus diaphysis to provide maximum tensile and compressive strains. Since the impact will be applied at the diaphysis middle, two gauges are placed on the upper face midway between the contact point and the end of the useful length of the bone (gages 1 and 2) and three other on the lower face respectively facing the two first gauges and the point of contact as shown in Figure 1*b*. Data recorded using a digital oscilloscope and filtered using CFC 1000 low pass filer to remove high frequency component. After instrumentation, the system humerus-brackets was scanned using a 3*D* scanner VIVID 910 KONICA

MINOLTA VI910 (0.1 *mm* of resolution) in order to obtain detailed description of boundary conditions as well as the precise locations of the gages in order to perform comparison with the Finite Element model.

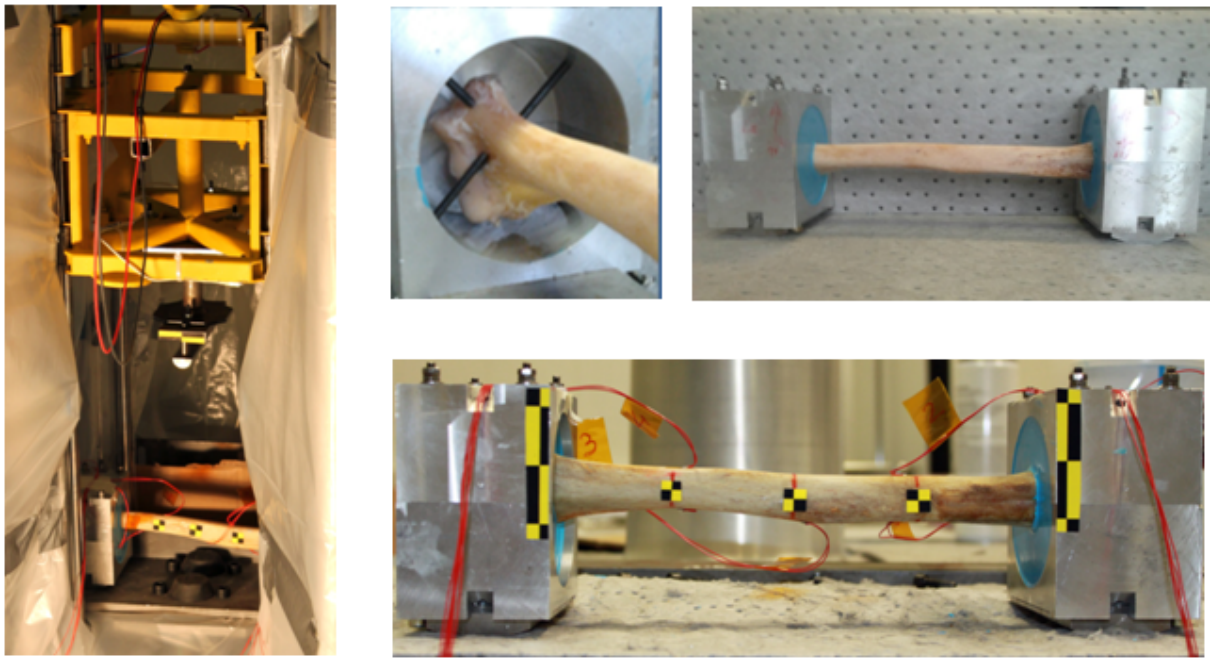

a) Drop tower device

b) Humerus preparation and instrumentation

Figure 1: Experimental device used for the bending impact on the human humerus

Three-points bending experiments were carried out using a drop tower impact apparatus of 2.30 *m* height. A drop mass fixed to a carriage was allowed to fall freely while guided on vertical rails. The carriage height can be adjusted to adapt the impact velocity (see Figure 1*a*). A laser sensor M7L was fixed to the drop tower bed in order to record the successive positions of the impactor. The humerus instrumentation together with high speed camera (3000 fps) provides a precise recording of the evolution of the impact load as well as the displacements/strain curves function of time.

2.1.2. Static bending experiments

First, static three-points bending experiments were performed on humeri diaphysis using several loads (carriage mass 1 *kg*, 3 *kg*, 5 *kg*). The measured parameters are the local strains given by the five gages for each prescribed weight. A least squares minimization technique was performed in order to determine the elastic modulus by means of an inverse analysis which consists in fitting computed data to experimental measurements which leads to optimal set of constitutive parameters (longitudinal Young's modulus in our case).

In Table 1 are listed the geometrical parameters and the mean estimates of the apparent longitudinal Young modulus for each humerus. As it can be observed, the average longitudinal elastic modulus is 19089.8 MPa with a standard deviation of 3082.78 MPa. This estimation fits within the average values given by [39; 25; 33]. We can also observe that the humerus 582 exhibits the lowest value of the elastic modulus. This is probably due to the low mass of this humerus.

Table 1: Mechanical properties of human humeral bone obtained from static loading

Humerus ID	Length (mm)	Mass (g)	Elastic modulus (MPa)
535	325	250	18954
514	361	354	19614
517	355	305	22445
485	331	262	14099
582	351	184	20337

Figure 2 represents the stress-strain curves of the five humeri based on the estimated Young modulus by optimization procedure and the local strain measurement of all three tensile gages Within this load range, the static response of each humerus was always linear.

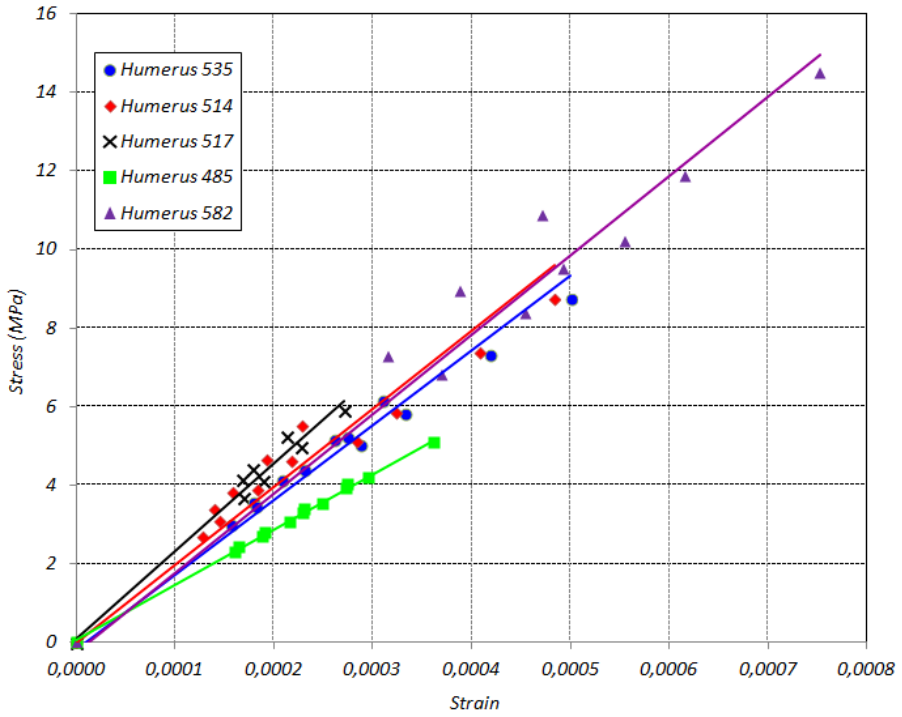

Figure 2: Experimental response of the humerus bones under static bending

2.1.3. Dynamic bending experiments

The dynamic impact experiment on the humerus was chosen to hit in the middle of the diaphysis with a projectile of 8.6 kg mass and 20 mm diameter. A drop height of 750 mm was used to generate an initial velocity of 1.63 m/s at the impact instant. The total impact energy of the present experiment was adjusted to be approximately $10J$. This value was shown from previous works [7], to be necessary to reach the human humerus ultimate strength. The impact load was measured using a 4 components load cell sensor (model KISLTER 9327A). A laser sensor was used to measure the displacement. The humerus instrumentation together with two high-speed video cameras provide a precise recording of the evolution of the impact load as well as the displacements/strain curves function of time.

The comparison between all humerus responses shows that only one humerus which did not break under the impacting load at the imposed initial velocity of 1.67 m/s.
Table 2 summarizes data obtained from the dynamic bending experiments. It can be noticed that the average bending stiffness (defined as the load divided by the deflection) of all specimens was about 465.6 N/mm with a standard deviation of 132.8 N/mm.

Regarding the humerus ultimate impact load, its average value was 1299.6 N with a standard deviation of 274.24 N. This value is consistent with the results presented by Duprey *et al.* [7] who found a mean maximum force value of 1273 N with a standard deviation of 448 N obtained using dynamic bending tests on humerus with an average velocity of 1.77 m/s. One can also cite the work of Mukherjee *et al.* [25] who performed dynamic bending tests on the shoulder bones using three different impact velocities. The mean ultimate impact load of humerus bones corresponding to the lower impact velocity considered was about 1275 N with a standard deviation of 671.75 N. This ultimate impact load increased naturally with the increasing of the impact velocity.

Table 2: Mechanical properties of human humerus bone for impact experiments

Humerus ID	Velocity (m/s)	Energy (J)	Bending stiffness (N/mm)	Ultimate impact load (N)
535	1.67	11.99	541	1592
514	1.63	11.42	642	1342
517	1.67	11.99	473	1239
485	1.65	11.71	344	1456
582	1.72	12.72	328	869

2.1.4. Densitometric measurements

Quantifying regional heterogeneities in bone characteristics such as the density might improve our understanding of the injuries mechanism of the extremity fractures. Few studies investigate the regional variation of the density of cadaver long bone. We can cite the densitometric measurements of Boos *et al.* [4] in 14 cadaver tibias who found that the mean bone densities varied between 123.79 mmg/mm^3 and 267.99 mmg/mm^3. For the humerus bone, Boos *et al.* [4] showed that the mean bone mineral density of the metaphysis region was 0.91 ± 0.224 g/cm^3, and the one of the epiphysis was 0.559 ± 0.139 g/cm^3.

In this study, densitometric measurements were performed after each dynamic test at the useful length of the impacted humerus in order to determine the porosity f of the diaphyseal cortical bone of the humerus. After removing brackets and strain gages, the humeri were cleaned from the bone marrow, cut into 8 zones (z_1 to z_8) and weighted using a precision weighing balance from OHAUS company (Figure 3). Then, the true density d_t were calculated from specimens weights in air and inside water by means of the Archimedes principle.

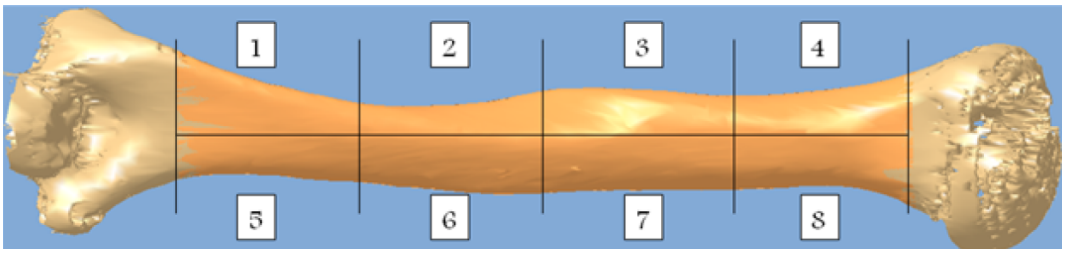

Figure 3: Specimens localization on the humerus

In Table 3 are listed true densities of each zones of the humerus bones. It can be observed that the mean true densities d_t varied between 1.69 g/cm^3 and 1.89 g/cm^3 showing the existence of interindividual differences. Moreover, regarding the same humerus, there is also intraindividual variances with respect to the eight zones.

Table 3: True densities of human humerus bone (g/cm^2)

Humerus ID	z_1	z_2	z_3	z_4	z_5	z_6	z_7	z_8	Mean	SD
535	1.79	1.84	1.87	1.75	1.71	1.90	2.17	1.79	1.85	0.14
514	1.87	1.92	1.81	1.79	1.86	1.95	1.86	1.51	1.82	0.13
517	1.66	1.93	1.88	1.75	1.87	2.35	1.90	1.80	1.89	0.20
485	1.56	1.76	2.36	1.67	1.85	1.81	1.78	1.70	1.81	0.23
582	1.83	2.13	1.84	1.80	1.98	1.89	1.53	1.84	1.86	0.17

Finally, the porosity of cortical bone was obtained using the relation $f = 1 - d_r$ where d_r is the relative

density defined as the ratio of the apparent density d_a by the true density d_t of the bone. The average porosity value of the diaphyseal cortical bone of the humerus was found to be equal approximately to 0.09.

2.2. Micromechanical characterization of the elastic properties

The heterogeneous and hierarchical nature of the diaphyseal cortical bone of the humerus makes it unlikely for a single measurement to fully characterize its structural integrity or accurately predict fracture risk. Hence, this study aims to understand the contributions of architecture and material properties on the elastic behavior by means of nanoindentation experiments. The well-known principle of nanoindentation lies in bringing a very small tip to the surface of the bone to make an imprint. Elastic modulus and hardness of the material are extracted from experimental readings of indenter load and depth of penetration.

Three small specimens were dissected from the humerus diaphysis and were milled down to a prismatic shape of $8 \times 5 \times 2mm$. The sampling area is located in the humerus distal part and is considered quite far from the rupture zone and has no apparent damage (Figure 4). Two of samples are intended for measures in the longitudinal direction of the humerus. The third one was intended for measures in the radial direction. These specimens were mechanically polished by an automatic grinding machine having off-centered rotating movements in order to achieve smooth and flat surface with substantially smaller roughness compared to indentation depths.

At first an abrasive polishing is applied with hydration using ultra-pure water and discs of different grain sizes 800, 1200, 2400 and 4000. Every polishing stage was done is 120 s with a rotary speed of 100 rpm. A final polishing with a felt disk coupled to a suspension of alumina particles of size 0.02 μm was then performed. This last polishing stage was applied with a fixed rotary speed of 100 rpm during 360 s. At the end an ultrasound rinsing bath was applied using ultra-pure water during 5 mn.

Figure 4: Bone specimens holder for polishing stage and nanoindentation experiments

After this preparatory step, nanoindentation tests were performed with a nanoindenter $G200$ from AGILENT using a Berkovich tip and the method proposed by Mazeran *et al.* [22]. This method is based on four stages protocol (loading, first 300s hold plateau, partial unloading and second 300s hold plateau) in order

to exhibit the time-dependent reversible and irreversible behavior. For each specimen, 40 indents were carried out in order to reduce the error associated with the measurement of the standard deviation. As nanonidentation experiments are conducted with pyramidal indenters, a quadratic dependence between load and displacement can be found. The relation between load F and indentation depth h is given by:

$$F = \frac{2}{\pi} E_r h^2 \tag{1}$$

E_r is the reduced modulus which relied to the bone elastic properties (E and ν fixed to 0.3) and the indenter elastic properties (E_i = 1141 GPa and ν_i = 0.07 for diamond material) by the relation:

$$\frac{1}{E_r} = \frac{1-\nu^2}{E} + \frac{1-\nu_i^2}{E_i} \tag{2}$$

The load versus indentation depth curve were fitted in the figure 5 using the quadratic rheological model performed by Mazeran *et al.* [22; 23] for the determination of bone mechanical properties.

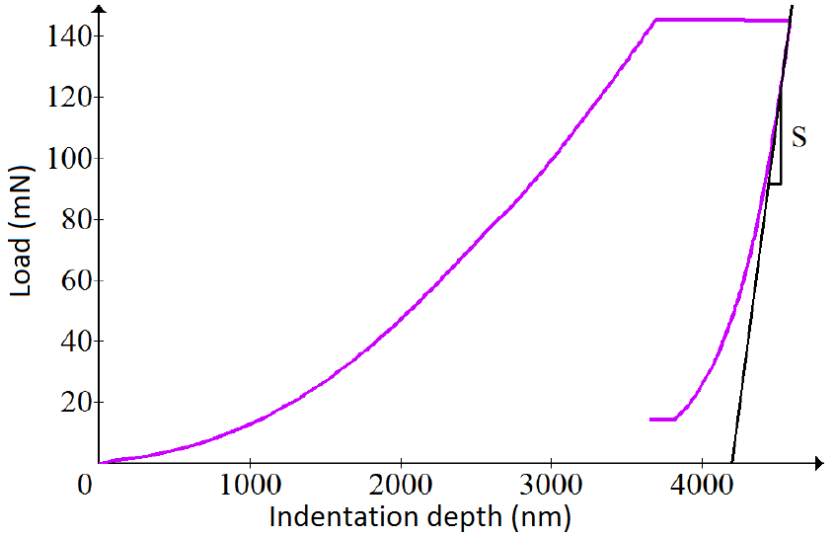

Figure 5: Load as function of the indentation depth

The results of this experimental campaign have provide mean values of the cortical bone elastic modulus of 19.50 ± 0.28 *GPa* in the longitudinal direction and of 18.6 ± 2.8 *GPa* in the transverse direction [41]. Moreover, the third specimen was tested on two localizations (the osteons and the interstitial tissues). The results showed mean values of the cortical bone elastic modulus of 18.2 ± 2.4 *GPa* for in the osteons tissue and of 21.1 ± 2.98 *GPa* in the interstitial tissue.

The average of the micromechanical elastic modulus denoted by E_m for infinite strain rate derived from

nanoindentation tests on the specimens of the humerus diaphyseal cortical bone has been found to be equal to 19.2 ± 3.1 GPa which fits within the average values available in the literature (see [41]).
It has to be noticed that the micromechanical Poisson ratio denoted by ν_m was not studied in the present investigation, its value was fixed to 0.3 as commonly proposed for long bones in the literature (see [3; 29]).

3. Theoretical formulation of the micromechanics based model of the diaphyseal humerus bone

In this section, the micromechanical modeling of the elastic behavior of the diaphyseal cortical bone of the humain humerus will be presented.

The diaphyseal cortical bone of the human humerus, in the present investigation, was considered as a porous media with a matrix phase weakened by micro-pores and exhibits transversely isotropic symmetry. The representative elementary volume REV of the bone is composed of an isotropic linear elastic solid matrix with stiffness $\mathbb{C}^m$ and of a set of cylindrical shaped pores having an elasticity tensor $\mathbb{C}^p$ and volume fraction f. The pores were taken to be identical in shape and orientation which characterized by a normal unit vector denoted by $\underline{n}$ (see Figure 6).

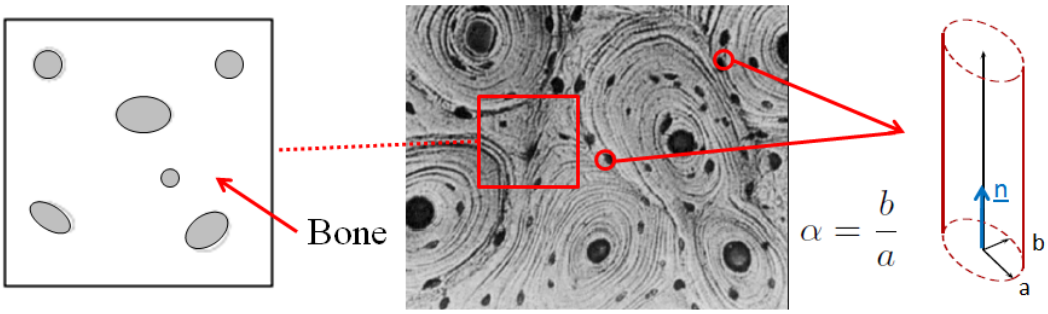

Figure 6: Description of the representative elementary volume

Taking advantage of the solution of the Eshelby equivalent inclusion problem [9; 18], the Mori-Tanaka homogenization scheme [24] provides the following expression of the homogenized elastic stiffness tensor for the porous media (see [27; 30; 31] for more detail):

$$\mathbb{C}^{hom} = \mathbb{C}^m + f\Big[(\mathbb{C}^p - \mathbb{C}^m)^{-1} + \mathbb{P}\Big]^{-1} : \Big[(1-f)\mathbb{I} + f\Big[\mathbb{I} + \mathbb{P} : (\mathbb{C}^p - \mathbb{C}^m)\Big]^{-1}\Big]^{-1} \tag{3}$$

where $\mathbb{I}$, $I_{ijkl} = \frac{1}{2}(\delta_{ik}\delta_{jl} + \delta_{il}\delta_{kj})$ is the fourth-order symmetric identity tensor and δ_{ij} is the Kronecker delta symbol. $\mathbb{P}$ is the Hill tensor [13] which depends on the shape and orientation of the pores (considered here as cylindrical voids of elastic stiffness tensor $\mathbb{C}^p = 0$) and on the elastic stiffness of the solid matrix $\mathbb{C}^m$.

We model the void as an infinite cylinder aligned along the $e_3 = \underline{n}$ (rectangular cartesian coordinate) axis, and of elliptical cross-section of aspect ratio $\alpha = \dfrac{b}{a}$ geometrically prescribed by:

$$\frac{x_1^2}{a^2} + \frac{x_2^2}{b^2} \leq 1, \quad -\infty < x_3 < +\infty \tag{4}$$

The determination of the Hill tensor $\mathbb{P}$, which is based on the work of [13] (see also [18; 37]), consists in evaluating the integral:

$$P_{ijpq} = \frac{\alpha}{2\pi} \int_{|\underline{\xi}|=1} \frac{\xi_i [K^m(\underline{\xi})]^{-1}_{jp} \xi_q \Big|_{(ij)(pq)}}{\xi_1^2 + \alpha^2 \xi_2^2} ds(\underline{\xi}) \tag{5}$$

for which the integration is on the unit circle centered at the origin of space (ξ_1, ξ_2), defined by $| \underline{\xi} | = 1$. $K^m_{ip}(\underline{\xi}) = C^m_{ijpq} \xi_j \xi_q$ is called the acoustic tensor. The notation $\Big|_{(ij)(pq)}$ indicates the symmetrization with respect to the couples (i, j) and (p, q).

The analytical evaluation of the tensor $\mathbb{P}$ is not an easy task. For transversely isotropic materials, it is interesting for standard notations and the associated tensorial representations to introduce the Walpole's base [38] which is constituted of a set of direction-related fourth-order tensors $\mathbb{E}^i$, $i = 1, .., 6$. By using this algebra and for cylindrical pores oriented with respect to the $e_3 = \underline{n}$ axis, Walpole's components of the Hill tensor $\mathbb{P}$ are given by [18; 38]:

$$\mathbb{P} = (2\kappa_p, n, 2\mu_p, 2\mu_n, l, l) \tag{6}$$

where κ_p, l, n, μ_p and μ_n the plane-strain bulk modulus, cross modulus, axial modulus under uni-axial strain, axial-shear modulus, and transverse-shear modulus, respectively. These components may be integrated analytically and are given in Appendix Appendix A.

Thus, for cylindrical voids of elliptical cross-section in an isotropic medium, we obtain the following expression of the longitudinal Young's modulus which it is independent of the aspect ratio α.

$$E_n = \frac{9\kappa^m \mu^m (1-f)}{3\kappa^m + \mu^m} \tag{7}$$

Moreover, if we consider that the aspect ratio is $\alpha = 1$ (the case of circular cylindrical voids), the transversal Young's modulus reads as:

$$E_p = \frac{18\kappa^m \mu^m (1-f)(3\kappa^m + \mu^m)}{9f\kappa^m(3\kappa^m + 4\mu^m) + 2(3\kappa^m + \mu^m)^2} \tag{8}$$

Making the same assumption of circular cylindrical voids, the components of the homogenized elastic stiffness tensor $\mathbb{C}^{hom}$ have been computed by means of the equation (3) and reported in Appendix Appendix B.

Finally, the obtained micromechanical model is implemented in a VMAT within the explicit dynamics code ABAQUS© for the prediction of the mechanical response of the humerus bone under low velocity impact. This model needs three materials parameters: the matrix elastic modulus E_m obtained by the nanoindentation tests, the diaphyseal cortical bone porosity f deduced from the densitometric measurements of the humerus bones and the matrix Poisson ratio ν_m given by the literature.In order to limit the number of unknown material parameters in this investigation, the aspect ratio is taken $\alpha = 1$, which corresponds to the assumption of cylindrical voids having a circular cross section.

4. Multi-scale Finite Element model of a human humerus bone under impact

4.1. 3D mesh generation of the humerus

The selected human humerus to be analyzed was the Humerus 517 which did not fail under the impact of an energy of $10J$. Therefore, it is assumed that this humerus exhibited an elastic behavior without damage nor failure and therefore it could be modeled using the present micromechanical elastic model.

The first step of the elaboration of the Finite Element (FE) model was the generation of the $3D$ CAD geometry of the humerus diaphysis by starting from the digitalized STL standard format. As shown in Figure 5a, the digitalized STL mesh was split into two different parts which represent the inner and outer surfaces of the humerus. Each STL surface was, partitioned along the transverse direction into 10 small parts (Figure 7a) using CATIA© CAD software. Then, small local surfaces were built up using their edges generated previously by CATIA© CAD facilities. Once the total inner and outer surfaces of the humerus diaphysis were reconstituted, a first mapped FE shell mesh model was generated using only quads. Then, a $3D$ mesh of the humerus volume was extruded using 7920 hexahedrons, thanks to the 3D meshing facilities available in HYPERMESH© software [1] (Figure 7b).

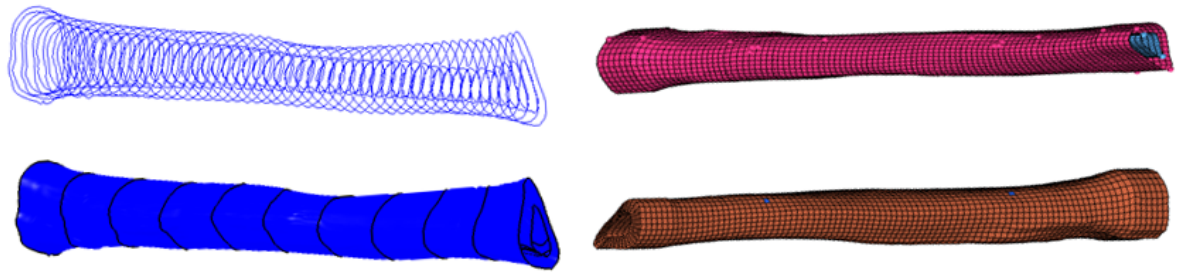

a) Humerus CAD geometry b) Humerus FE mesh

Figure 7: Humerus Finite Element model

4.2. *Modeling of the drop tower impact on the humerus*

The final stage of this investigation was the elaboration of the FE model including boundary conditions, material parameters, contact and loading conditions, in order to simulate the impact bending of the humerus and try to validate the material model. To this purpose, two brackets with concentrated mass elements of 1080 g have been modeled using hexahedral elements with the assumption of a rigid elastic material. The center of mass of each rigid bracket was allowed to move along the X-axis and to rotate around the Y-axis as shown in Figure 8. The humerus epiphyses were embedded into the brackets using a prismatic shaped solid of $71 \times 71 \times 55$ mm and having the resin material parameters ($\rho = 1500\ kg/m^3$, $E = 400\ MPa$, $\nu = 0.3$). For the sake of biofidelity, the inner part of the humerus diaphysis was filled by a solid representing the marrow with elastic properties $E = 1\ MPa$, $\nu = 0.3$ and $\rho = 1000\ Kg/m^3$ (see [14]). The system brackets-humerus was positioned on a plate of $400 \times 150 \times 10$ mm size and of $10,77$ kg mass which has been modeled as an analytical rigid body.

The impactor was considered as a cylindrical shell of 20 mm diameter and 8.6 kg of mass. It has been modeled using S4R shells of ABAQUS© elements and a rigid elastic material (see Figure 8). All contact interfaces were modeled using "General Contact" conditions without friction. The FE simulation was carried out using a total duration of 10 ms to cover the entire impact process. The 3D mesh of the whole FE system includes 7920 C3D8R solid elements and analytical solid. The FE simulation was carried out using the Explicit Dynamics algorithm of ABAQUS© software.

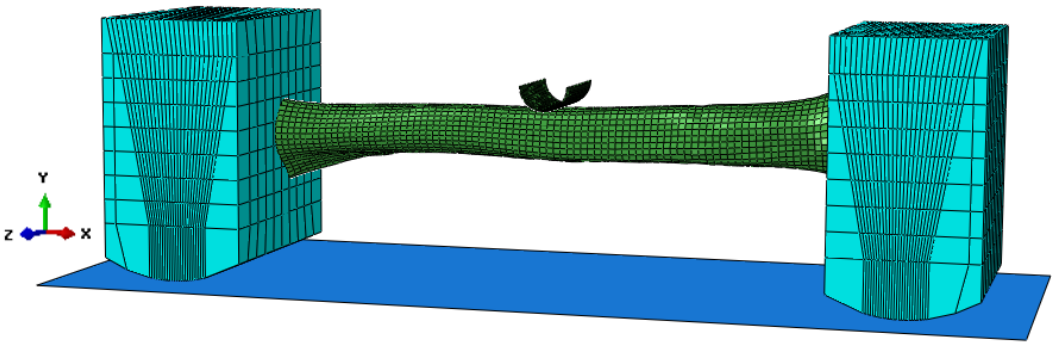

Figure 8: Drop tower modeling using Finite Element method

4.3. *Analysis of the material parameters influence*

In order to analyze the influence of materials parameters on the FE simulation of the humerus elastic response under bending impact, different set of parameters are considered. Figure 9 represents the load-displacement curves of the modeled humerus 517 under three values of porosity, matrix modulus, longitudinal and transverse elastic moduli. As can bee seen in Figure 9(a), the increased cortical porosity f

rendered lower structural stiffness as well as lowered peak force along with an increased ability to absorb energy before failure. On the other hand, we have studied in Fig. 9(b) the variation of the matrix elastic modulus E_m around its mean value determined by nanoindentation experiments. We notice that an increase in matrix elastic modulus is correlated with an increase of bone elastic properties namely the bending stiffness. The same phenomenon occurs for the longitudinal elastic modulus E_n at fixed transverse one E_p (Fig. 9(C). However, there was no detectable effect of the variation of the transverse elastic modulus on the elastic response of the humerus when the longitudinal elastic modulus was fixed (see Fig. 9(d)). For the next

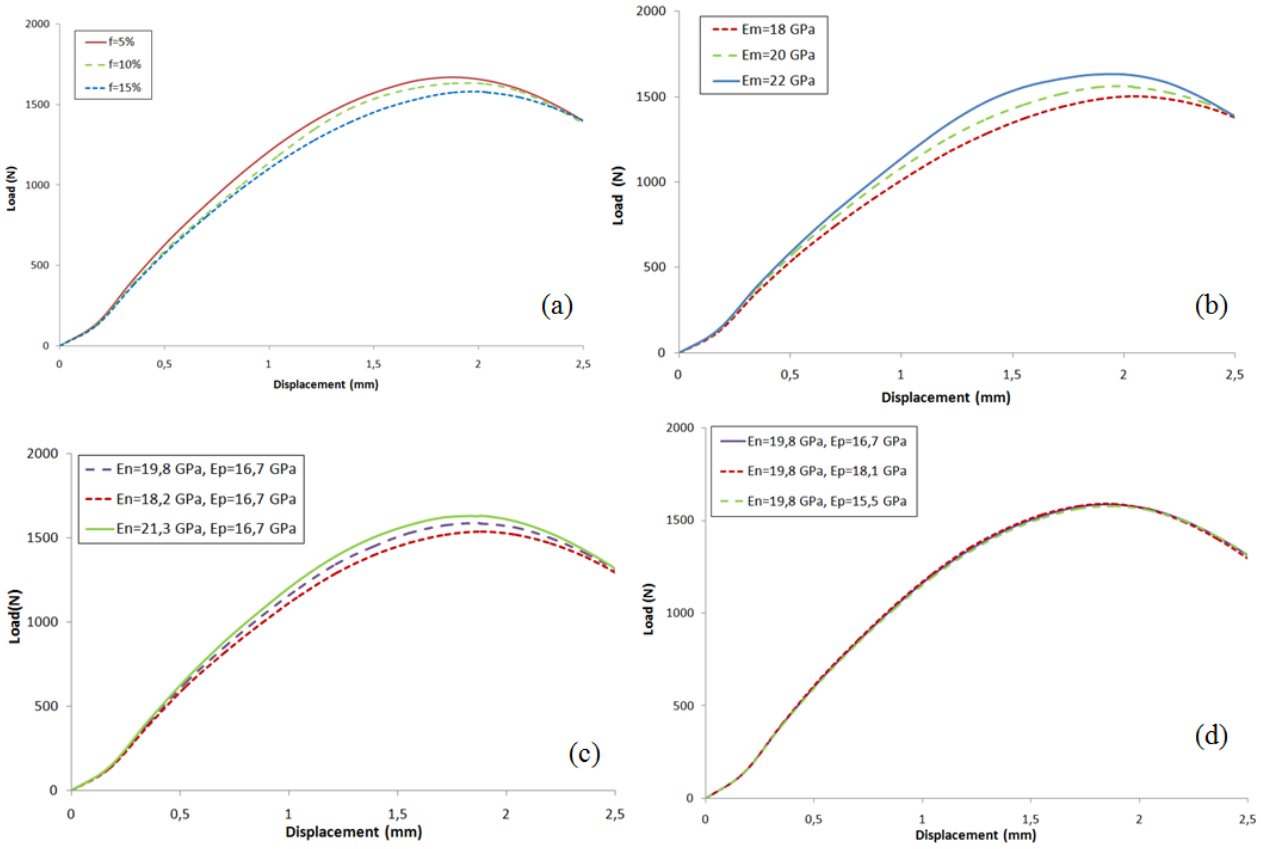

Figure 9: Influence of humerus material parameters on the load-displacement curves : (a) porosity, (b) matrix modulus, (c) Longitudinal modulus, (d) transverse modulus

of study, the material parameters used in FE simulations of the humerus 517 are $E_m = 19.2\ MPa$, $\nu_m = 0.3$ and $f = 0.09$.

5. Discussion

This study was performed for the mechanical characterization of the elastic behavior of the human humerus under impact using a newly developed multi-scale model. The originality of the proposed approach consists

in the identification of only few material parameters to describe the whole complex anisotropic behavior of the humerus bone.

To investigate the effect of the impact velocity on the elastic response of the humerus under bending impact, three different velocities (1.5, 1.77 and 1.9 m/s) were applied. As we can show in Figures 10(a) and 10(b), the impact velocity affected clearly the elastic properties of the humerus. An increasing of the impact velocity leads naturally to an increasing of bending stiffness and strain.

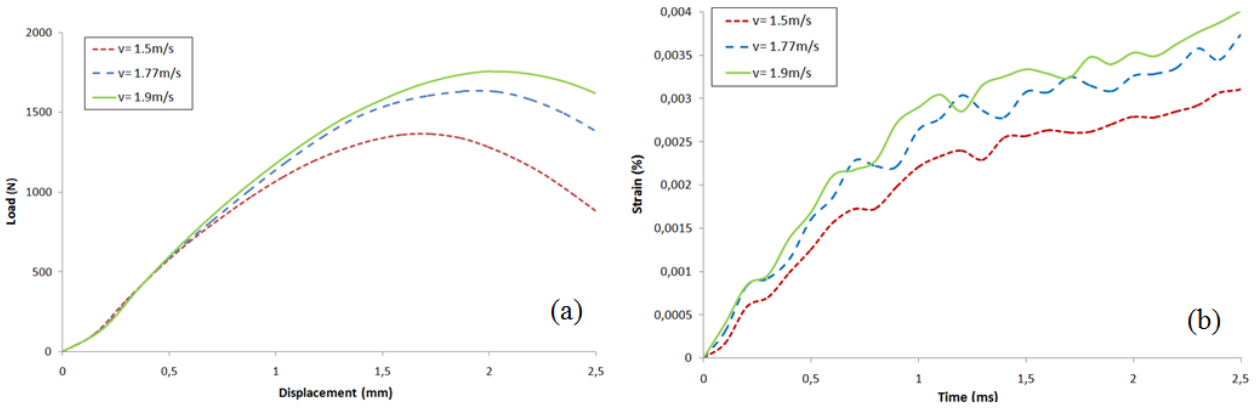

Figure 10: Effect of the impact velocity : (a) load versus displacement curve, (b) strain versus time curve

Figure 11 shows the evolution of humerus response under the impact load. One can observe globally an overall good agreement in the estimation of ultimate load in comparing the predicted numerical solution to the various experimental responses. From Table 3, one can notice that the micromechanical model gives an ultimate impact load of 1201 N with a minimum error of 7% [33].

The comparison between experimental measurements and the numerical predictions of the impact load shows that the predicted ultimate load is somehow under-estimated, this is probably due to the local bone material identification. Indeed, it has been reported [20] that nano-indentation experiments often induce damage into the bone prior to the physical measure, therefore the resulting elastic characteristics are often underestimated even if the embalming solution has a small effect on Young's modulus and other properties measured in static tests. However, some authors [10; 40] found that impact energy absorption seems to be reduced by quite a large amount, and that results of high strain rate tests may be more affected than the results of static tests. Nevertheless the remaining minor deviations could be simply attributed to the natural differences in geometry (size and morphology) between all tested humeral bones, which is common for most of biological materials [2].

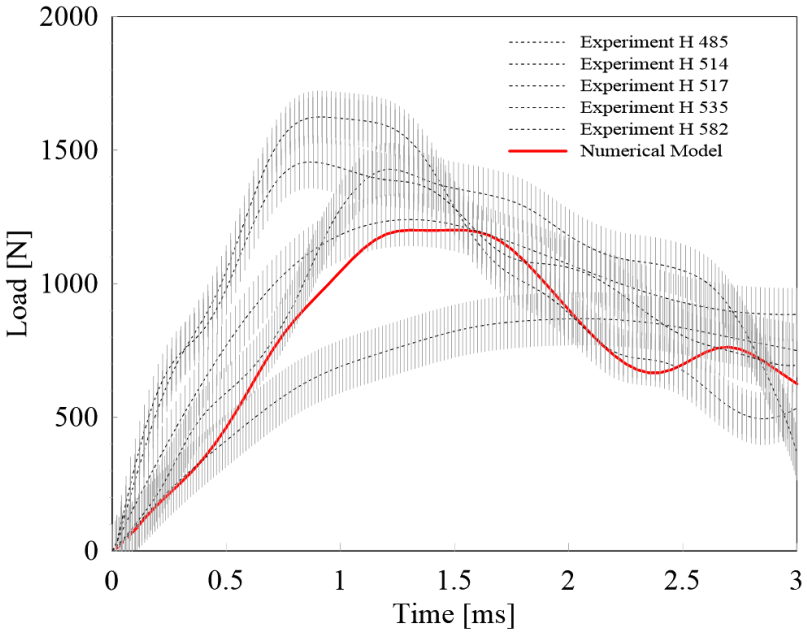

Figure 11: Mechanical response of the humerus under impact loading (experiment vs numerical)

However, despite the aforementioned experimental uncertainties, one can remark that the obtained ultimate impact load shows a relatively limited error (7%) compared to the mean experimental measured load. The same remark can be made regarding the instant necessary to reach the ultimate force (1.35 ms), which is very close to the mean experimental one (1.40 ms) (Table 4).

Moreover, the strain response of strain-gauge-acquired values at the mid-diaphysis of human humeri was investigated. At this location, the maximum strain values ranged from 0.25% to 0.97% with an average experimental value of 0.66 ± 0.17. The error of the mean measured maximum strain from the FE-calculated maximum strain was found to be equal to 3%. This minimum error assesses the performance of the Finite Element model in capturing the true humerus bone response for the three-point bending tests.

Table 4: Comparison of the ultimate impact load and maximum strain of the modeled humerus (Numerical vs. Experiment)

	Load (N)	Time (ms)	Maximum strain (%)
FE Model	1201	1.35	0.64
Experiment (mean)	1299	1.40	0.66
Error Model	7%		3%

These results seem promising for future applications such as evaluation of injury risk in lateral car crashes [19]. As the proposed model can utilize detailed numerical representations of the human humerus with

accurate geometric and material properties, a perspective is to realize a geometric personalization of the model. This would allow the assessment of the influence of a model personalization. In addition, this humerus model can be integrated in a whole-body model for applications such as shoulder lateral impacts. It can be subjected to a given loading condition, producing response characteristics intended to mimic the human body in a real world scenario. The primary advantage of human body models, however, is that they provide insight into the onset of injury and resultant local response characteristics thereafter through the use of stress and strain data measured throughout the entire model. Such information is unobtainable during volunteer or post mortem human subject testing. These models remove the issue of repeatability, allowing for the implementation of parametric studies often used by vehicle designers to improve automotive safety.

6. Conclusions

In conclusion, the framework of homogenization was proposed for the modeling of elastic behavior for diaphyseal cortical bone. The elastic properties of the human humerus were investigated by coupling the Mori-Tanaka scheme and the micromechanical measurements of the cortical bone properties using nanoindentation experiments.

The proposed model predicts adequately the experimental results via the estimation of the ultimate impact load that the humerus may encounter before fracture. Further improvements will be performed to the present model to be able to simulate the bone fracture by taking into account the nonlinear behavior and including the strain rate effects and effective fracture criteria.

7. Acknowledgments

The authors gratefully acknowledge the financial support from the French Ministry of Research

Appendix A. Hill tensor for elliptic cylindrical inclusions

The Hill tensor for cylindrical inclusions of elliptical cross-section with the aspect ratio α embedded in an isotropic solid matrix, can be written, by using (6), in the form:

$$2k_p = \frac{\alpha}{1+\alpha}\frac{3}{(3\kappa^m + 4\mu^m)}, \quad n = 0, \quad 2\mu_p = \frac{\alpha}{(1+\alpha)^2}\frac{3\kappa^m + \mu^m(3\alpha+4)}{\mu^m(3\kappa^m + 4\mu^m)}, \quad 2\mu_n = \frac{1}{1+\alpha}\frac{1}{2\mu^m}, \quad l = 0 \tag{A.1}$$

where κ^m and μ^m are the bulk and shear moduli of the bone matrix.

Appendix B. Elastic stiffness tensor for circular cylindrical inclusions

The Walpole's components of the homogenized stiffness tensor of the humeral bone are :

$$\mathbb{C}^{hom} = (2\kappa_p^{hom}, n^{hom}, 2\mu_p^{hom}, 2\mu_n^{hom}, l^{hom}, l^{hom})$$

where:

$$C_{1111} = \kappa_p^{hom} + \mu_p^{hom}, \quad C_{1122} = \kappa_p^{hom} - \mu_p^{hom}, \quad C_{2323} = \mu_n^{hom}, \quad C_{3333} = n^{hom}, \quad C_{1133} = l^{hom}$$

The non-zero components of the homogenized elastic stiffness tensor for cylindrical inclusions of circular cross-section (the case of aspect ratio $\alpha = 1$) and of volume fraction f in an isotropic medium can be calculated analytically, by using (3) and (A.1) and are written as:

$$\begin{cases} C_{1111} = C_{2222} = \dfrac{\mu^m(1-f)(3\kappa^m+\mu^m)(2f+1)(3\kappa^m+4\mu^m)}{(3\mu^m+f\mu^m+3f\kappa^m)(3\kappa^m+\mu^m+3f\kappa^m+7f\mu^m)} \\ C_{1122} = \dfrac{\mu^m(1-f)(3\kappa^m+\mu^m)(3\kappa^m-2\mu^m+6f\mu^m)}{(3\mu^m+f\mu^m+3f\kappa^m)(3\kappa^m+\mu^m+3f\kappa^m+7f\mu^m)} \\ C_{1133} = C_{2233} = \dfrac{\mu^m(3\kappa^m-3f\kappa^m-2\mu^m+2f\mu^m)}{3\mu^m+f\mu^m+3f\kappa^m} \\ C_{3333} = -\dfrac{\mu^m(-3\kappa^m-6f\kappa^m-4\mu^m+4f\mu^m+9f^2\kappa^m)}{3\mu^m+f\mu^m+3f\kappa^m} \\ C_{2323} = C_{1313} = \dfrac{2\mu^m(1-f)}{1+f} \\ C_{1212} = -\dfrac{\mu^m(-3\kappa^m-6f\kappa^m-4\mu^m+4f\mu^m+9f^2\kappa^m)}{3\kappa^m+\mu^m+3f\kappa^m+7f\mu^m} \end{cases} \tag{B.1}$$

References

[1] Altair Engineering (2010) HyperMesh© 10.0 User's Guide. Altair Engineering Inc.. World Headquarters 1820 E. Big Beaver Rd. Troy MI 48083-2031 USA.

[2] Aziz MSR, Nicayenzi B, Crookshank MC, Bougherara H, Schemitsch EH, Zdero R (2014) Biomechanical Measurements of Stiffness and Strength for Five Types of Whole Human and Artificial Humeri. Journal of Biomechanical Engineering, 136(5):1-10.

[3] Baca V, Horak Z, Mikulenka P, Dzupa V (2008) Comparison of an inhomogeneous orthotropic and isotropic material models used for FE analyses. Medical Engineering and Physics. 30 : 924-930.

[4] Boosa C, Fink K, Stomberg P, Köller W, Igl BW, Russlies M (2007) The intraindividual agreement of the bone density of the human proximal tibia. AnnALs of anatomy, 189:515519.

[5] Carrera EF, Nicolao FA, Archetti Netto N, Carvalho RL, dos Reis FB, Giordani EJ (2008) A mechanical comparison between conventional and modified angular plates for proximal humeral fractures. Journal of Shoulder and Elbow. Surgery Board of Trustees, 631-636.

[6] Clavert P, Javier R-M, Charrissoux JL, Obert L, Pidhorz L, Sirveaux F, Mansat P, Fabre T (2016) How to determine the bone mineral density of the distal humerus with radiographic tools?. Surgical and Radiologic Anatomy, 38:389393.

[7] Duprey S, Bruyere K, Verriest JP (2007) Experimental and simulated flexion tests of humerus. International Journal of Crashworthiness 12(2):153-158.

[8] Elie-Dit-Cosaque X, Gakwaya A, Naceur H (2014) Smoothed finite element method implemented in a resultant eight-node solid-shell element for geometrical linear analysis. Computational Mechanics, 1-22.

[9] Eshelby JD (1957) The determination of the elastic field of an ellipsoidal inclusion and related problems. Proceedings of the Royal Society Series A 252:561-569.

[10] Gauthier R, Follet H, Langer M, Meille S, Chevalier J, Rongiéras F, Peyrin F, D Mitton (2017) Strain rate influence on human cortical bone toughness: A comparative study of four paired anatomical sites. Journal of the Mechanical Behavior of Biomedical Materials, 71:223-230.

[11] Van Haaren EH, Van der Zwaard BC, Van der Veen AJ, Heyligers IC, Wuisman PJ, Smit TH (2008) Effect of long-term preservation on the mechanical properties of cortical bone in goats. Acta Orthopaedica 79 (5):708716.

[12] Hellmich C, Barthelemy J, Dormieux L (2004) Mineral-collagen interactions in elasticity of bone ultrastructure-a continuum micromechanics approach. Eur. J. Mech. A Solids 23:783-810.

[13] Hill R (1965) A self-consistent mechanics of composite materials. Journal of the Mechanics and Physics of Solids, 13:213-222.

[14] Ho K-Y, Keya JH, Powers CM (2014) Comparison of patella bone strain between females with and without patellofemoral pain : a finite element analysis study. Journal of Biomechanics 47(1):230-236.

[15] Hoffler CE, Moore KE, Kozloff K, Zysset PK, Brown MB, Goldstein SA (2000) Heterogeneity of bone lamellar-level elastic moduli. Bone, 26(6) 603-609.

[16] Hungerer S, Wipf F, von Oldenburg G, Augat P, Penzkofer R (2014) Complex Distal Humerus FracturesComparison of Polyaxial Locking and Nonlocking Screw ConfigurationsA Preliminary Biomechanical Study. Journal of Orthopaedic Trauma, 28(3):130-136.

[17] Kaufman R, Fraade-Blanar L, Lipira A, Friedrich J, Bulger E (2017) Severe soft tissue injuries of the upper extremity in motor vehicle crashes involving partial ejection: the protective role of side curtain airbags. Accident Analysis and Prevention, 102:144-152.

[18] Laws N, McLaughlin R (1979) The effect of fiber length on the overall moduli of composite materials. Journal of the Mechanics and Physics of Solids 27:1-13.

[19] Lebarbé M, Vezin P, Rongiéras F, Lafont D (2017). Human Shoulder Response to High Velocity Lateral Impact. Stapp Car Crash Journal, 61:27-51.

[20] Malandrino A, Fritsch A, Lahayne O, Kropik K, Redl H, Noailly J, Lacroix D, Hellmich C (2012). Anisotropic tissue elasticity in human lumbar vertebra, by means of a coupled ultrasound-micromechanics approach. Materials Letters, 78:154-158.

[21] Marques M, Belinha J, Oliveira AF, Natal Jorge RM (2019) Chapter 10: Determination of the Anisotropic Mechanical Properties of Bone Tissue Using a Homogenization Technique Combined With Meshless Methods. Advances in Biomechanics and Tissue Regeneration, 201-213.

[22] Mazeran P-E, Beyaoui M, Bigerelle M, Guigon M (2012) Determination of mechanical properties by nanoindentation in the case of viscoelastic materials. International Journal of Material Research, 103:715-722.

[23] Jaramillo Isaza S, Mazeran P-E, El Kirat K, Ho Ba Tho M-C (2014). Time-dependent mechanical properties of rat femoral cortical bone by nanoindentation: An age related study. Journal of Material Research, 29:1135-1143.

[24] Mori T, Tanaka K (1973) Averages stress in matrix and average elastic energy of materials with misfitting inclusions. Acta Metallia. vol. 21:571-574.

[25] Mukherjee S, Chawla A, Borouah S, Sahoo D, Arun MWJ (2011) Dynamic properties of the shoulder complex bones. Society

of Automotive Engineers, 11-17.

[26] Naceur H, Shiri S, Coutellier D, Batoz JL (2013) On the modeling and design of composite multilayered structures using solid-shell finite element model. Finite Elements in Analysis and Design 70:1-14.

[27] Naceur H, Rahmoun J, Halgrin J, Chabrand P (2015) Multiscale finite element modeling of ductile damage behavior of the human femur under dynamic loading. International Journal of Damage Mechanics, 24:418-445.

[28] Ohman C, DallAra E, Baleani M, Van Sint Jan S, Viceconti M (2008) The effects of embalming using a 4% formalin solution on the compressive mechanical properties of human cortical bone. Clinical Biomechanics, 23:1294-1298.

[29] Peng L, Bai J, Zeng X, Zhou Y (2006) Comparison of isotropic and orthotropic material property assignments on femoral finite element models under two loading conditions. Med Eng Phys, 28(3):227-233.

[30] Rahmoun J, Chaari F, Markiewicz E, Drazetic P (2009) Micromechanical modeling of the anisotropy of elastic biological composites. Multiscale Modeling and Simulation, 8 (1):326-336.

[31] Rahmoun J, Auperrin A, Delille R, Naceur H, Drazetic P (2014) Characterization and micromechanical modeling of the human cranial bone elastic properties. Mechanics Research Communications, 60:7-14.

[32] Santos B, Quental C, Folgado J, Sarmento M, Monteiro J (2018) Bone remodelling of the humerus after a resurfacing and a stemless shoulder arthroplasty. Clinical Biomechanics, 59:78-84.

[33] Singh D, Rana A, Jhajhria SK, Garg B, Pandey PM, Kalyanasundaram D (2019) Experimental assessment of biomechanical properties in human male elbow bone subjected to bending and compression loads. Journal of Applied Biomaterials and Functional Materials, 1-13.

[34] Stefan U, Michael B, Werne S (2010) Effects of three different preservation methods on the mechanical properties of human and bovine cortical bone. Bone, 47:1048-1053.

[35] Toop T, Muller T, Huss S, Kann PH, Weihe E, Ruchloltz S, Peter R (2012) Embalmed and fresh frozen human bones in orthopedic cadaveric studies: which bone is authentic and feasible? Acta Orthopaedica, 39 (5):543547.

[36] Vandenbulcke F (2015) Caractérisation et modélisation multi-échelle du comportement mécanique à la rupture du membre scapulaire sous sollicitations dynamiques. PhD Thesis University of Valenciennes.

[37] Willis JR (1977) Bounds and self-consistent estimates for the overall moduli of anisotropic composites. Journal of the Mechanics and Physics of Solids 25:185-202.

[38] Walpole LJ (1969) On the overall elastic moduli of composite materials. Journal of the Mechanics and Physics of Solids 12:235-251.

[39] Yamada H (1970) Strength of biological materials. F G Evans (Ed.), Baltimore, MD, Williams and Wilkins.

[40] Zhai X, Gao J, Nie Y, Guo Z, Kedir N, Claus B, Sun T, Fezzaa K, Xiao X, Chen WW (2019) Real-time visualization of dynamic fractures in porcine bones and the loading-rate effect on their fracture toughness. Journal of the Mechanics and Physics of Solids, 131:358-371.

[41] Zysset PK, Edward Guo X, Edward Hoffler C, Moore KE, Goldstein SA (1999) Elastic modulus and hardness of cortical and trabecular bone lamellae measured by nanoindentation in the human femur. Journal of Biomechanics, 32(10):1005-1012.